Optical and Quantum Electronics (2020) 52:208
https://doi.org/10.1007/s11082-020-02323-7

High-density quantum bits generation using microring plasmonic antenna

A. E. Arumona[1,2,3] · I. S. Amiri[4] · S. Punthawanunt[5] · P. Yupapin[1,2]

Received: 12 November 2019 / Accepted: 23 March 2020

Abstract
Plasmonic antenna in the form of the panda-ring circuit proposed, which consists of a silicon microring with two side nanorings, from which the silicon microring embedded by a gold grating. The gold grating generated polariton which results in oscillation of plasmonic wave with plasma frequency, from which the center wavelength shifted to the Bragg wavelength. The Bragg wavelength at resonance applied for all calculations. By using suitable parameters, the whispering gallery mode obtained, which is the consequence of trapping of light inside the silicon microring. In manipulation, the input light of 1.50 μm center wavelength fed into the system. The input power varied from 3 to 15 mW. The electron densities are trapped and transported either by cable connection or wireless connection making use of the whispering gallery mode. For the space–time function, the space function signal is the dark soliton, which fed into the panda-ring circuit through the input port. The space–time function was multiplexed using the modulated Gaussian pulse through the add port where the signals multiplexed by signals of higher frequency circulating within the system. These results in the formation of the flip flop (clock) signal as well as the spin up and spin down signals which can transmit via dual-mode operation. By using the spin projection modulation control, the transmission bit rates of ~ 40 Pbit s^{-1} is achieved.

Keywords Silicon microring circuit · High density quantum bits · Quantum communication · Plasmonic electronics

✉ P. Yupapin
preecha.yupapin@tdtu.edu.vn

A. E. Arumona
arumonaarumonaedward.st@student.tdtu.edu.vn

[1] Computational Optics Research Group, Advanced Institute of Materials Science, Ton Duc Thang University, District 7, Ho Chi Minh City, Vietnam

[2] Faculty of Applied Sciences, Ton Duc Thang University, District 7, Ho Chi Minh City, Vietnam

[3] Division of Computational Physics, Institute for Computational Science, Ton Duc Thang University, Ho Chi Minh City 700000, Vietnam

[4] Division of Materials Science and Engineering, Boston University, Boston, MA 02215, USA

[5] Faculty of Science and Technology, Kasem Bundit University, Bangkok 10250, Thailand

Published online: 02 April 2020

1 Introduction

Plasmonic materials are usually gold, silver, and graphene, which are nanostructured and known to be optical (dielectric) nanoantenna (Yousif and Samra 2013; Hadadi et al. 2016; Prateekha and Dinesh 2019; Yuan-Fong et al. 2016a, b; Chua et al. 2013). The plasmonic antenna usually made from these metals, where the plasmon waves from by the interaction between free electrons on the metals and incident light. The optical radiation freely propagating is converted into localized energy and vice versa (Novotny and van Hulst 2011; Yuan-Fong et al. 2019; Wayne et al. 2013). The plasmonic antenna operates in the optical frequency, which is a high-frequency regime where the penetration of the electromagnetic field through the metal at a depth called skin depth. The effect of the skin depth illuminated by light the inertial of the conduction electrons increased, which results in a delay in their response. The light incident the metal modelled the electrons which couples to the electron plasma, resulting in the formation of rapid oscillation. From which the metallic electrons respond relative to the incident beam and plasma wavelengths (Youplao et al. 2018; Karnetzky et al. 2018; Atabaki et al. 2018; Gaetano et al. 2017). The plasmonic antenna has various forms of different designs, where one of them is the panda-ring circuits (Bunruangses et al. 2019; Shahidinejad et al. 2013; Arumona et al. 2020). It consists of silicon microring (Radjenović et al. 2017; Milanovic et al. 2012) with two nanorings at the sides of the silicon microring. It can use for the dual-mode operation, where the operation modes such as wireless or cable connections can apply. When it is a wireless connection, the whispering gallery mode is employed. The whispering gallery mode is the consequence of trapping and squeezing of light inside a microring. This phenomenon can observe in silicon microring due to the nonlinearity effect exhibited by the microring. Whispering gallery mode (WGM) has many applications, in which many researchers have used this phenomenon for various studies (Punthawanunt et al. 2018; Khomyuth et al. 2018; Trong and Chang 2017). Another mode is operated by cable connection, in which the signals transmitted by the fiber network. Pons-Valencia et al. (2019) used the plasmonic antennas to launch hyperbolic phonon polaritons (HPhPs) in thin h-BN slabs which enhanced molecular spectroscopy and photodetection. Ummethala et al. (2019) used the plasmonic modulator in converting data streams from wireless communication at THz to optical domain in a fiber-optic network. Vahid et al. (2019) made use of plasmonic nanoantennas that crossed shaped for solar cell applications. Mohammad et al. (2019) designed a photoconductive dipole antenna using a gold plasmonic nanodisk array. The quantum efficiency of the photoconductive antenna enhanced as a result of plasmonic excitation. Vahid and Mahrdad (2019) proposed a new design of plasmonic nanoantenna that has a bow-tie shape. The plasmonic antenna is useful for tunable broadband, where the strong electric field applied. Pengfei et al. (2019) used the plasmonic antennas to enhance Nickel(II) ions catalysis that is, the plasmonic antenna absorbs light that is visible intensely resulting in hot electrons produced at the surface which generates an electromagnetic field that is localized. This property used in enhancing the Nickel(II) cation catalytic performance. In this work, the plasmonic antenna formed by panda-ring embedded a gold grating circuit applied for quantum bits generation and transmission, where the spin projection control applied by the modulated function. The Optiwave program employed where the whispering gallery mode formation in the microring obtained. The panda-ring circuit acts as a plasmonic antenna makes use of dual-mode operation where the whispering gallery mode is used as a wireless link called light

fidelity (LiFi) network and as cable network making use of the optic fibre network. The parameter extracted from the Optiwave program used by the Matlab program making use of space–time function for quantum bits transmission.

2 Background

The plasmonic antenna in the form of a panda-ring circuit shown in Fig. 1, where the panda-ring consists of silicon microring embedded with gold gratings at the centre. The gold gratings illuminated that light produces electrons described by the Drude model (Derkachova and Kolwas 2007; Tunsiri et al. 2019; Prince 2018). The relationship between the plasma frequency and electron density given by an Eq. (1).

$$\epsilon(\omega) = 1 - \frac{ne^2}{\epsilon_0 m\omega^2} \tag{1}$$

where the electron density, relative permittivity, mass, electron charge are n, ϵ_0, m, e respectively. The angular frequency ω becomes plasma frequency (ω_p) at resonance, which is written by

$$\omega_p = \left[\frac{ne^2}{\epsilon_0 m}\right]^{-1/2} \tag{2}$$

From Eq. (2), the electron density $n = \frac{\omega_p^2 \epsilon_o m}{e^2}$. The plasmonic wave oscillation is a consequence of electron density in an electric field. Maxwell's equations give the TM-polarization along with exponential decay of the electric field.The Bragg wavelength is related to the wavelength at resonance as $\lambda_B = 2n_e\Lambda$, where n_e and Λ are the effective refractive index and grating period respectively. The effective refractive index represents the grating's refractive index in the waveguide. The nonlinear Kerr effect is given in terms of the refractive indices by $n = n_0 + n_2 \mathrm{I} = n_0 + n_2 P/A_{eff}$, where n_0 and n_2 are the linear and nonlinear refractive indices, respectively. Optical intensity and power are I and P respectively. The effective mode core area of the device is A_{eff}. The two

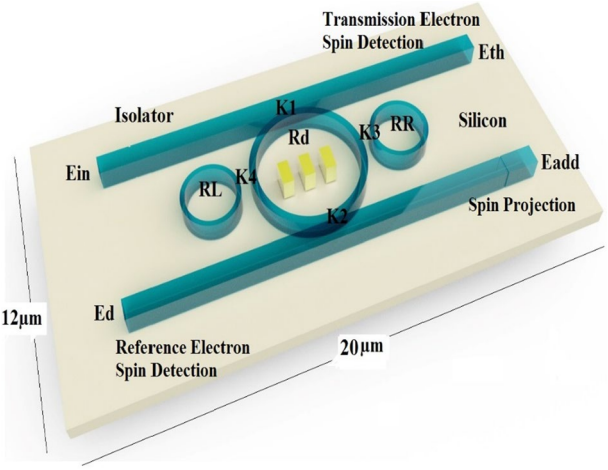

Fig. 1 Schematic of the proposed silicon microring circuit, where E_{in}: input port, E_{th}: throughput port, E_{add}: add port and E_d: drop port. R_d: main ring radius, R_R and R_L: side ring radii, K1–K4: coupling constants. The isolator and spin projection control are applied to protect the feedback and filtering purpose. The reference electron spin detection at the drop, the transmission electron spin detection at the throughput port, and spin projection control applied at the add port

nanorings at the sides of the silicon microring act as phase modulators, which control the whispering gallery mode at resonance and through the throughput and drop ports the normalized intensities are obtained. The normalized intensities are written by

$$\frac{I_{th}}{I_{in}} = \left[\frac{E_{th}}{E_{in}}\right]^2 \tag{3}$$

$$\frac{I_{drop}}{I_{in}} = \left[\frac{E_{drop}}{E_{in}}\right]^2 \tag{4}$$

The dark soliton is a space function applied as the input source to drive the gold grating force, while the modulated Gaussian pulse used as the modulation source, which can offer the unified space–time configuration for spin control application. From which the infinitesimal of the phase modulators can arrange the space–time uncertainty saturation, where space–time the singularity obtained when the space–time uncertainty saturation achieved. The input field is the dark soliton which is given by an Eq. (5) (Agrawal 2011).

$$E_{in} = B \cdot Tanh\left(\frac{T}{T_0}\right)\exp\left(\frac{z}{2L_D}\right) \tag{5}$$

where λ_1 is the input dark soliton wavelength, which is specified as the first space-function, where B and z are amplitude and propagation distance, respectively. T is the time of propagation of the soliton pulse in a frame moving with group velocity, L_D is the length dispersion, where $L_D = \frac{T_0^2}{\beta}$, where T_0 is the initial propagation time. β is the propagation constant in linear and nonlinear terms.

The Gaussian pulse is used as the modulated source, which is given as:

$$E_{add} = De^{\pm i2\pi\left(\frac{c}{\lambda_2}\right).t} \tag{6}$$

where λ_2 is the wavelength of the space–time input. $D, candt$ are the amplitude, speed of light in the vacuum, and time respectively. The $\pm$ sign of the exponent term used for the full-time slot axis, which can apply to have the spin control given by $e^{\pm i\omega t}$ and t = 0 for spin-up and down, respectively.

From Eq. (6) it can be rewritten by an Eq. (7).

$$E_{add} = De^{\pm i\omega_2 t_2} \tag{7}$$

where $\omega_2 = 2\pi\gamma_2$, $\gamma_2 = \frac{c}{\lambda_2}$. ω_2 is the angular frequency, and γ_2 is the linear frequency. The quantum transmission signal is the multiplexed functions of the input and add port signals, which is written by $Be^{-i\left(\omega_2 t_2 + \frac{E_n}{n\hbar} t_3\right)}$. Where $B = \overline{B} \cdot \text{Tanh}\left(\frac{T}{T_0}\right)\exp\left(\frac{z}{2L_D}\right)$, which is the dark soliton (space function). By using the synchronous multiplexing condition, then $t = t_2 = t_3$. $\omega_2 t_2$ is the phase tm of the multiplexing function, which can set as the initial input that can be vanished. $\frac{E_n}{n\hbar_h}$, n = 1, 2, 3,… from Eq. (7) the spin number is $\pm\frac{\hbar}{2}$, $\hbar$ is the reduced Planck's constant. $\hbar = \frac{h}{2\pi}$. and h is the Planck's constant. In manipulation, the spin term will present by the full-time slot of the electron transport, where the spin-up and down of the electron cloud can be distinguished and applied.

3 Results and discussion

In the simulation, the plasmonic antenna in the form of a panda-ring circuit shown in Fig. 1. The input light source of 1.50 μm center wavelength fed into the system through the input port, from which the gold grating is excited by the input light which results in the oscillation of the plasmonic wave and polariton at a wavelength called the Bragg wavelength. The whispering gallery mode made is possible formed by the coupling of light inside the microring with the embedded gold gratings at the center of the silicon microring. The gold grating is responsible for the shifting of the center wavelength to the Bragg wavelength. The output signals are usually obtained at the throughput and drop ports. Firstly, in the manipulation, the 32-bit version 12.0 (OptiFDTD 2019) of the Optiwave FDTD program is used and at resonance with a particular wavelength results in the trapping of light inside the silicon microring. The Optiwave FDTD simulation has a grid size of 0.05 for Δx, Δy, and Δz respectively. The APML (anisotropic perfect matched layer) is employed in the boundary condition with an APML layer of 15, real tensor of 1.0 and 1.0×10^{-12} theoretical reflection coefficient. The dimension of the simulation model is 274, 49 and 314 mesh cell size in the x, y, and z-axis, respectively. The total number of 20,000 round trips used to confirmed resonant results. A high-performance computer of 32 Gb RAM used for all simulations to ensure accuracy. As shown in Fig. 2, the WGM formed at the centre of the silicon microring using other parameters in Table 1. The plot of the ratio of the throughput and drop ports with the varied input power from 3 to 15 mW is shown in Fig. 3. The results showed a linear trend as the power varied with three different grating periods. For the first grating period ($\Lambda1=0.50$ μm) there is a sharp increase in the output value at the drop port as the power changes from 10 to 15 mW due to the reflection of the input light at this high input power. The parameters extracted from the first simulation that is, the results of the Optiwave FDTD simulation and used in the Matlab program. From Fig. 4, the WGM of the resonant output with the outputs at the throughput and drop ports plotted in the time, wavelength and frequency domains. The centre wavelength of 1.50 μm shifted to the Bragg wavelength of 1.59 μm by the gold gratings at the centre of the silicon microring. The plot of the time function shown in Figs. 5 and 6. The output signals at the throughput and drop ports are shown, from which the throughput port is the bright soliton, while the drop port is the dark soliton. The trapped electron cloud (density) formed by the bright and dark soliton envelops. This kind of scenario is also known as a flip-flop, where the bright soliton is assigned the logic value of 1 while the dark soliton is assigned the logic value of 0. By using the spin projection control, the trapped electron cloud and no spin projection of ~4 Pbit s^{-1} achieved as shown in Figs. 5 and 6. The LHS (left-hand side) is spin-down (red), RHS (right-hand side) is spin-up (blue) of Throughput port with the bit rate of ~ 40 Pbit s^{-1} achieved. LHS is spin-down (red), RHS is spin-up (blue) of Drop port with a bit rate of ~ 40 Pbit s^{-1} achieved. The quantum transmission can confirm by the electron spin

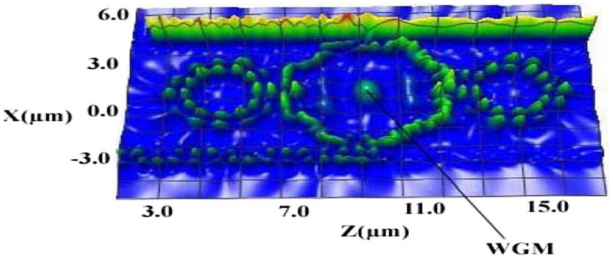

Fig. 2 Graphical results obtained by the Opti-wave program, where the used output is the whispering gallery mode (WGM) at the centre ring of the circuit, where R = 2.0 μm, R_R = 1.0 μm, R_L = 1.0 μm, each κ = 0.50, Input power = 15 mW, with the center wavelength of 1.50 μm, and other parameters given in Table 1

Table 1 The selected parameters of the system used in the simulation

Parameters	Symbols	Values	Units
Input power (Bright soliton)	P	3–15	mW
Input power (Gaussian pulse)	P	3–15	mW
Si-linear waveguide length	L	16.0	μm
Si center ring radius	R	2.0	μm
Si small ring radius	R_L	1.0	μm
Si small ring radius	R_R	1.0	μm
Gold dielectric constant (Pornsuwancharoen et al. 2017)	ϵ_0	6.9	
Gold permittivity (Pornsuwancharoen et al. 2017)	ϵ	10.0	
Gold thickness	d	0.1	μm
Gold length	L	0.5	μm
Gold refractive index (Pornsuwancharoen et al. 2017)	n	1.80	
Coupling coefficient	κ	0.50	
Insertion loss	γ	0.01	
Refractive index Si (Prabhu et al. 2010)	n_{Si}	3.42	
Si nonlinear refractive index) (Prabhu et al. 2010)	n_2	1.3×10^{-13}	$m^2\ W^{-1}$
Input light wavelength input port	λ_1	1.50	μm
Modulation wavelength input (Space–time function)	λ_2	1.30	μm
Waveguide core effective) (Prabhu et al. 2010)	A_{eff}	0.30	μm^2
Waveguide loss	α	0.50	dB (cm^{-1})
Plasma frequency (Blaber et al. 2009)	ωp	1.2990×10^{16}	rad s^{-1}
Electron mass	m	9.11×10^{-31}	kg
Electron charge	e	1.6×10^{-19}	Coulomb
Permittivity of free space	ϵ_0	8.85×10^{-12}	F m^{-1}
Reduced Planck's constant	$\hbar$	1.00	ARU
Planck's constant	h	2π	ARU
Grating period	Λ	0.50, 0.40, 0.30	μm

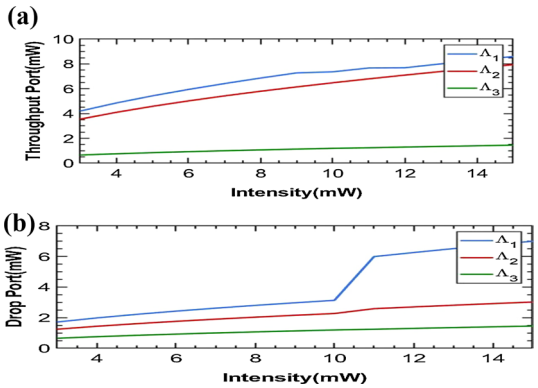

Fig. 3 The plot of the ratio of the **a** throughput port/input signal, **b** drop port/input port at different grating periods. $\Lambda_1 = 0.50$ μm, $\Lambda_2 = 0.40$ μm, $\Lambda_3 = 0.30$ μm

entanglement plot, which shown in Fig. 7. The initial phase degree of 0°–90° applied for clarity, which zoomed from 50°–90°. The input power varied from 3 to 15 mW shown in Fig. 6a–c. By using an Eq. (8), the plot of the spin number results is shown in Fig. 8, where

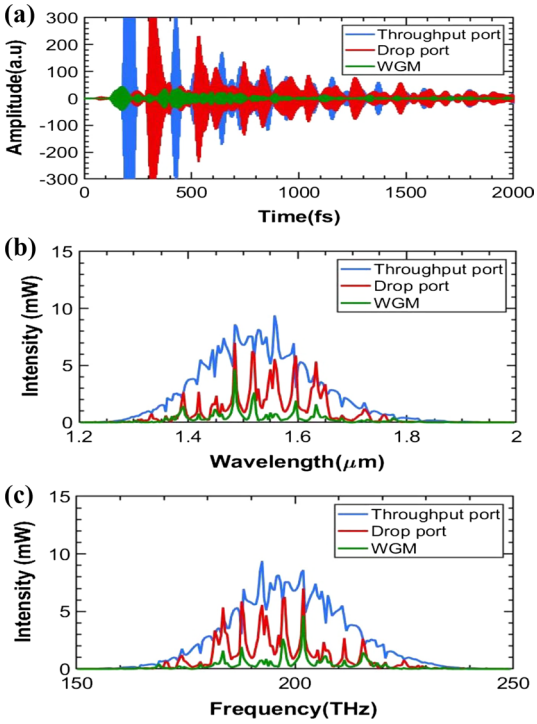

Fig. 4 Shows the plot of the output at the throughput port signal, where drop port and the WGM signals at the centre system (grating) were **a** time-domain, **b** wavelength domain and **c** frequency domain. The Bragg wavelength is 1.59 μm applied for plasma frequency calculation

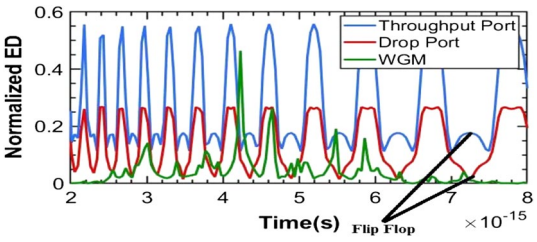

Fig. 5 The plot of the Matlab program results using the time function for the throughput port, drop port and WGM. The orthogonal electron clouds obtained, where the bit rates of ~ 4 Pbit s^{-1} achieved, in which the high-density and stability quantum bits generation obtained

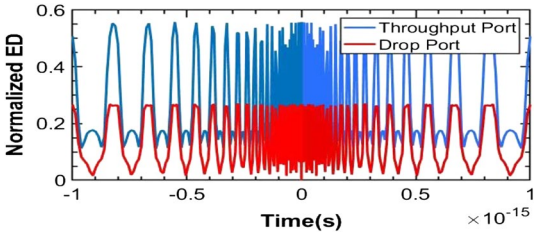

Fig. 6 The plot of the Matlab program for the time function, where the spin-up and down at the throughput port (blue), at the drop port (red), where the spin packet switching formed with the full-time slot projection. The throughput port output with bit rate of ~ 40 Pbit s^{-1} achieved. The drop port output with bit rate of ~ 40 Pbit s^{-1} achieved

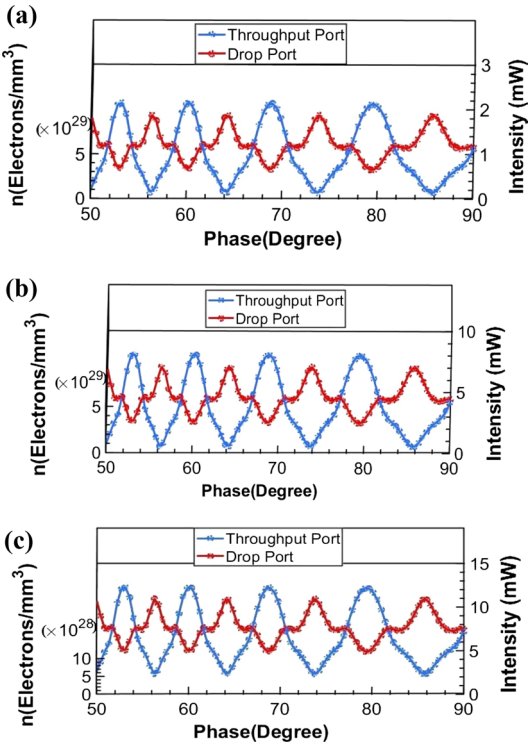

Fig. 7 The plot of the Matlab program for the entanglement of the output at the throughput and drop ports with electron density where **a** using the power of 3 mW, **b** using the power of 10 mW and **c** using the power of 15 mW. The consistence of the reference and transmitted quantum bits obtained, which can related by the classical channel via Alice and Bob confirmation

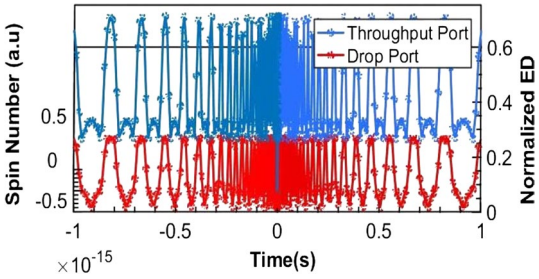

Fig. 8 The plot of the Matlab program for the spin number, where spin-up and down the throughput (blue) port and drop port (red), where the spin packet switching formed with the full-time slot projection. The throughput port output with bit rate of ~ 40 Pbit s^{-1} achieved. The drop port output with bit rate of ~ 40 Pbit s^{-1} achieved

the spin-up at the throughput port and the spin-down at the drop port. The spin packet switching obtained, which is useful for high-density quantum bits and quantum cellular automata applications. The LHS (left-hand side) is spin-down (red), RHS (right-hand side) is spin-up (blue) of Throughput port with bit rate of ~ 40 Pbit s^{-1} achieved. LHS is spin-down (red), RHS is spin-up (blue) of Drop port with bit rate of ~ 40 Pbit s^{-1} achieved. The high-density quantum bits can generate and transmit via the spin-wave transmission, where the spin states distinguished by the time sequence, which is known as a quantum cellular automata transmission (Wiesner 2009; Trailokya et al. 2018). The spin packet switching signals of the transmitted and referenced electron cloud can apply for high density quantum bits transmission. The electron cloud at the center is high density due to the intense optical power and shown by the electron cloud distributed results due to the applied input power in Fig. 3. The high-density quantum bits can transmit via the spin-wave and detect

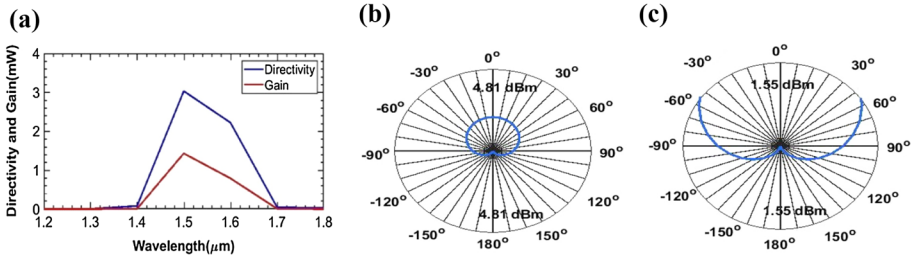

Fig. 9 The plot of the plasmonic antenna profile of the center ring, where **a** the directivity and gain at the center wavelength, **b**, **c** are the plasmonic antenna directivities

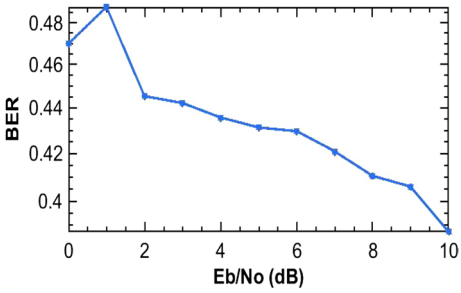

Fig. 10 The plot of the BER calculation of the proposed transmission system, the BER value of 0.39 is obtained

by projection control, where the spin states distinguished by the time sequence, and useful for high-density bit rates transmission requirement. The electron spin number of the transmission (throughput) and the reference (drop) port, which can relate to the electron cloud during the quantum cellular automata processing and transmitted bits. In application, the panda-ring circuit can form the plasmonic antenna, which can apply in a quantum computing device, quantum sensor, quantum encryption and so much more.

The antenna profile of the present work is shown in Fig. 9. The plot of the directivity and gain at the center wavelength of 1.50 μm is shown in Fig. 9a, where the directivity is 3.03 mW, the gain is 1.43 mW. The plasmonic antenna directivity is 4.81 dBm, and the gain is 1.55 dBm, as shown in Fig. 9b, c. The directivity and gain are obtained, explained in Arumona et al. (2020). In principle, the Bragg wavelength formed, and plasmonic waves generated the plasma frequency. The gold grating generated the plasmonic polaritons and dipole oscillation at the center of the microring. The resonant light couples into the microring structure lead the wave propagating at the center microring, from which the plasmonic antenna is formed. The bit error rate (BER) is simulated for the data transmission of the system using the AWGN channel. Additive White Gaussian Noise (AWGN) is a communication channel model usually accompanied by noise. The signal to noise ratio of 10 dB is employed in the simulation, wherein the signal and noise are input into the transmission input. The input signals are modulated. The transmitted signals are demodulated and recovered signals retrieved at the end-user. The BER versus Eb/No (Energy per bit/noise spectral density) graph gives the indication or measures the number of errors or the errors in receiving the transmitted data. Figure 10 shows that the BER value gives the system's operational performance, where the higher BER, the lower the system's operational performance obtained. From the calculation, the BER value of 0.39 is obtained. The advantage of this system is the high bit of data transmission. This system transmitted ~ 40 Pb compared with

the following works: Benjamin et al. (2006) system transmitted 10Gbs^{-1}. Jianxun et al. (2017) system transmitted 160 Gb s^{-1}. Aref et al. (2018) system transmitted 9.04 Mb s^{-1}. Douwe et al. (2005) system transmitted 10 Gb s^{-1}. El-Fiky et al. (2017) system transmitted 168 Gb s^{-1}.

4 Conclusion

The plasmonic antenna in the form of the panda-ring circuit is proposed and manipulated for high-density quantum bits generation and transmission, which can apply for dual-mode operation by controlling the two side phase modulators. The dual-mode operation can either be wireless or cable connections. Principally, the polariton induced by the plasmonic waves generated by the incident photon to the gold grating at the centre of the silicon microring, which results in the oscillation of plasmonic wave at the Bragg wavelength. The polariton induced by the gold grating can be employed to form the plasmonic sensor and dipole oscillation. The transport of the trapped electron density within the circuit is made possible via wireless connection making use of the whispering gallery mode and via cable connection. The trapped electron densities can form the electron spins by the spin control projection function, which can detect and transmission at the drop and throughput ports. It is useful for spin-transmission via the spin-wave transmission. By using the full-time slot spin projection, the spin states can distinguish by the time sequence, which can apply for the quantum cellular automata processing. The working principle based on the space–time function synchronous multiplexing, in which the trapped electron densities can apply for the quantum electronics, spintronics and quantum computer, the generated electron spins can apply for various applications. The space–time function multiplexed by the modulated Gaussian pulse through the add port, where the higher frequency circulating within the system leading to the formation of the flip-flop (0, 1), spin up and spin down signals, in which the dual-mode operation can apply via the spin-wave carrier transmission. The required information can retrieve via the spin projection, where the confirmation between sender and receiver can confirm by the classical channel. The transmission bit rates of ~ 40,000 Tbit s^{-1} (40 Pbit s^{-1}) is achieved. By using the full-time slot projection, the quantum cellular automata using the individual electron spin recognition is also possible.

Acknowledgements One of the authors (Mr. Arumona) would like to thank the Ton Duc Thang University, Vietnam for their financial support.

References

Agrawal, G.P.: Nonlinear fiber optics: its history and recent progress [Invited]. J. Opt. Soc. Am. B **28**(12), A1–A10 (2011)

Aref, T., Mohamed, A., Ahmed, C.A., Yvon, S., Mohamad, S.: A 1.5 pJ/bit, 9.04 Mbit/s carrier-width demodulator for data transmission over an inductive link supporting power and data transfer. IEEE Trans. Circuits Syst. II Express Briefs **65**(10), 1420–1424 (2018)

Arumona, A.E., Amiri, I.S., Yupapin, P.: Plasmonic micro-antenna characteristics using gold grating embedded panda-ring circuit. Plasmonics **15**, 279–285 (2020)

Atabaki, A.H., et al.: Integrating photonics with silicon nanoelectronics for next generation of system on a chip. Nature **556**, 349–354 (2018)

Benjamin, G.L., Benjamin, A.S., Keren, B.: Transmission of high-data-rate optical signals through a micrometer-scale silicon ring resonator. Opt. Lett. **31**(18), 1–3 (2006)

Blaber, M.G., Arnold, M.D., Ford, M.J.: Search for the ideal plasmonic nanoshell: The effects of surface scattering and alternatives to gold and silver. J. Phys. Chem. C **113**, 3041–3045 (2009)
Bunruangses, M., Youplao, P., Amiri, I.S., Pornsuwancharoen, N., Yupapin, P.: Brain sensor and communication model using plasmonic microring antenna network. Opt. Quant. Electron. **51**, 349 (2019)
Chua, Y.F., Lin, W.H., Sung, M.J., Jheng, C.Y., Jheng, S.C., Tsai, D.P.: Numerical investigation of a castle-like contour plasmonic nanoantenna with operating wavelength ranging in ultraviolet-visible, visible light, and infrared light. Plasmonics **8**, 755–761 (2013)
Derkachova, A., Kolwas, K.: Size dependence of multipolar plasmon resonance frequencies and damping rates in simple metal spherical nanoparticles. Eur. Phys. J. Spec. Top. **144**, 93–99 (2007)
Douwe, G., Edwin, K., Henry, K., Nigel, B., Alfred, D.: Compact wavelength-selective switch for gigabit filtering in access networks. IEEE Photonics Technol. Lett. **17**(2), 336–338 (2005)
El-Fiky, E., Mathieu, C., Mohammed, S., Alireza, S., Morsy-Osman, M., David, V.P.: 168 Gb/s single carrier PAM4 Transmission for intra data center optical interconnects. IEEE Photonics Technol. Lett. **29**(3), 314–317 (2017)
Gaetano, B., Giovanna, C., Ali, E.K., Paolo, B., Vincenzo, P.: Integrated Vivaldi plasmonic antenna for wireless on-chip optical communications. Opt. Express **25**(14), 16214–16227 (2017)
Hadadi, T., Mohammed, N.M., Arezoomand, A.S., Zarrabi, F.B.: Sub wavelength plasmonic nano-antenna with modified ring structure for multi resonance application and circular polarization. Opt. Quant. Electron. **48**(20), 1–9 (2016)
Jianxun, H., Feng, Q., Xiaoyang, C., Andrew, M.S., Shiyoshi, Y.: A high-speed electro-optic triplemicroring resonator modulator. Sci. Rep. **7**(1), 1–6 (2017)
Karnetzky, C., Philipp, Z., Christopher, T., Carolina, D.S., Martin, W., Reinhard, K., Alexander, H.: Towards femtosecond on chip electronics based on plasmonic hot electron nano-emitters. Nat. Commun. **9**(1), 1–7 (2018)
Khomyuth, S., Mahdi, B., Amiri, I.S., Youplao, P., Pornsuwancharoen, N., Yupapin, P.: Electric-optic conversion circuit incorporating a fiber loop for light fidelity up-down link use. Microwave Opt. Technol. Lett. **61**(2), 526–531 (2018)
Milanovic, B., Radjenovic, B., Radmilovic-Radjenovi, M.: Three-dimensional finite-element modeling of optical microring resonators. Phys. Scr. **TI49**, 1–4 (2012)
Mohammad, K., et al.: Terahertz radiation enhancement in dipole photoconductive antenna on LT-GaAs using a gold plasmonic nanodisk array. Opt. Laser Technol. **120**, 105726 (2019)
Novotny, L., van Hulst, N.: Antennas for light. Nat. Photonics **5**, 83–90 (2011)
OptiFDTD Technical Background and Tutorials (Finite Difference Time Domain) Photonics Simulation Software, Version 12.0. https://www.optiwave.com, Searched on 20th Sept 2019.
Pengfei, H., Tana, T., Qi, X., Sarina, S., Eric, R.W., Daniel, E.G., Huaiyong, Z.: Promoting Ni(II) catalysis with plasmonic antennas. Chem **5**(5), 1–21 (2019)
Pons-Valencia, P., et al.: Launching of hyperbolic phonon-polaritons in h-BN slabs by resonant metal plasmonic antennas. Nat. Commun. **10**, 1–8 (2019)
Pornsuwancharoen, N., Amiri, I.S., Suhailin, F.H., Aziz, M.S., Ali, J., Singh, G., Yupapin, P.: Micro-current source generated by a WGM of light within a stacked silicon-graphene-Au waveguide. IEEE Photonics Technol. Lett. **29**(21), 1768–1771 (2017)
Prabhu, A.M., Alan, T., Zhanghua, H., Vien, V.: Extreme miniaturization of silicon add-drop microring filters for VLSI photonics applications. IEEE Photonics J. **2**(3), 436–444 (2010)
Prateekha, S., Dinesh, K.V.: Multilayer hybrid plasmonic nano patch antenna. Plasmonics **14**(2), 435–440 (2019)
Prince, G.: Controlling level splitting by strong coupling of surface plasmon resonances with rhodamine-6G on a gold grating. Plasmonics **13**(6), 2067–2077 (2018)
Punthawanunt, S., Aziz, M.S., Phatharacorn, P., Chiangga, S., Ali, J., Yupapin, P.: LiFi cross-connection node model using whispering gallery mode of light in a microring resonantor. Microsyst. Technol. **24**(12), 4833–4838 (2018)
Radjenović, B., Radmilović-Radjenović, M., Beličev, P.: Eigenmodes of finite length silicon-on-insulator microring resonator arrays. Opt. Quant. Electron. **49**, 1–17 (2017)
Shahidinejad, A., Ali, N., Toni, A., Ali, S.: Optical wireless quantum communication coding system using decimal convertor. Opt. Quant. Electron. **45**, 449–457 (2013)
Trailokya, N.S., Ashutosh, K.S., Anand, M.: An efficient design of quantum-dot cellular automata based 5-input majority gate with power analysis. Microprocess. Microsyst. **59**, 103–117 (2018)
Trong, H.B.N., Chang, Y.C.: Whispering gallery modes in hybrid Au-ZnO microsphere resonators: experimental and theoretical investigations. Opt. Mater. Express **7**(8), 2962–2967 (2017)
Tunsiri, S., Nopparat, T., Thanunchai, T., Somsak, M., Yupapin, P.: Microring switching control using plasmonic ring resonator circuits for super-channel use. Plasmonics **14**, 1669–1677 (2019)

Ummethala, S.S., et al.: THz-to-optical conversion in wireless communications using an ultra-broadband plasmonic modulator. Nat. Photonics **13**, 519–524 (2019)

Vahid, K., Mahrdad, S.S.: Increased electric field enhancement and broad wavelength tenability by plasmonic bow-tie nano-antenna based on fractal geometry with grid. Photonics Nanostruct. Fundam. Appl. **35**, 100705 (2019)

Vahid, K., Mojtaba, J., Mehrdad, S.S.: UV and IR cut off filters based on plasmonic crossed-shaped nanoantennas for solar cell applications. Opt. Commun. **433**, 275–282 (2019)

Wayne, Y., Yuan-Fong, C.C., Jheng, S.C.: Analysis of transmittance properties of surface plasmon modes on periodic solid outline bowtie nanoantenna arrays. Phys Plasmas **20**(6), 064503 (2013)

Wiesner, K.: Quantum cellular automata. In: Meyers, R. (ed.) Encyclopedia of complexity and systems science. Springer, New York (2009)

Youplao, P., Pornsuwancharoen, N., Amiri, I.S., Jalil, M.A., Aziz, M.S., Ali, J., Singh, G., Yupapin, P., Grattan, K.T.V.: Microring stereo on sensors model using Kerr Vernier effect for Bio-cell sensor and communication. Nano Commun. Netw. **17**, 30–35 (2018)

Yousif, B.B., Samra, A.S.: Optical responses of plasmonic gold nanoantennas through numerical simulation. J. Nanopart. Res. **15**(1), 1–15 (2013)

Yuan-Fong, C.C., Jhih-Cyuan, J., Chung-Ting, C.C., Hai-Pang, C., Chee, M.L.: Manipulating near field enhancement and optical spectrum in a pair-array of the cavity resonance based plasmonic nanoantennas. J. Phys. D Appl. Phys. **49**(47), 475102 (2016a)

Yuan-Fong, C.C., Chung-Ting, C.C., Jhin-Yu, R., Hai-Pang, C., Chee, M.L., Ren, C.L., Nyuk, Y.V.: Tunable optical performance on a periodic array of plasmonic bowtie nanoantennas with hollow cavities. Nanoscale Res. Lett. **11**(1), 411 (2016b)

Yuan-Fong, C.C., Chung, T.C.C., Hung, J.H., Ya-Chih, W., Hai-Pang, C., Muhammad, N.S.M.I., Zarifi, M., Chee, M.L.: Strong and tunable plasmonic field coupling and enhancement generating from the protruded metal nanorods and dielectric cores. Results Phys. **13**(102290), 1–8 (2019)